



*Supplement of*

**Sensitivity of climate–chemistry model simulated atmospheric composition to the application of an inverse relationship between NO<sub>x</sub> emission and lightning flash frequency**

Francisco J. Pérez-Invernón et al.

*Correspondence to:* Francisco J. Pérez-Invernón (fjpi89@gmail.com)

The copyright of individual parts of the supplement might differ from the article licence.

## S1. Introduction

We include in this supporting material additional figures illustrating the influence of the new parameterization of  $\text{LNO}_x$  production (Bucsela et al., 2019, Fig. 11(c)). in the chemistry of the atmosphere. The simulated annual average flash density during 2001 is shown in Figure S1. Figure S2 shows the annual spatial distribution of  $\text{LNO}_x$ . Figures S3-S11 show the annually and

5 globally averaged differences of the  $\text{NO}_x$ ,  $\text{O}_3$ ,  $\text{CO}$ ,  $\text{HO}_x$ ,  $\text{HNO}_3$  and  $\text{HNO}_4$  mixing ratios between the control simulations and the simulations using the new parameterization of  $\text{LNO}_x$  production at different pressure levels and by using different lightning parameterizations. Figures S12-S13 show the impact of  $\text{LNO}_x$  on the  $\text{HO}_x$  mixing ratio in the geographical region of

10 Europe (bounded by  $42^\circ\text{N}$  and  $52^\circ\text{N}$  latitude degrees, and  $0^\circ$  to  $24^\circ\text{E}$  longitude degrees) at the 200 hPa and the 600 hPa pressure levels, respectively. Figures S14-S25 show the monthly averaged total  $\text{O}_3$  column in 2004 from the control simulations.

10 Figures S26-S29 show the interannual zonally averaged differences (in %) during each season of the vertical  $\text{O}_3$  mixing ratio between the annual Bodeker scientific global vertically resolved ozone database Tier 1.4 vn1.0 product Hassler et al. (2009) and the annually mean during the period 2002-2007 of each season. Finally, Figure S30 is adapted from Jöckel et al. (2016), showing a comparison between the simulated and the observed climatological annual mean of observed tropospheric partial column ozone.

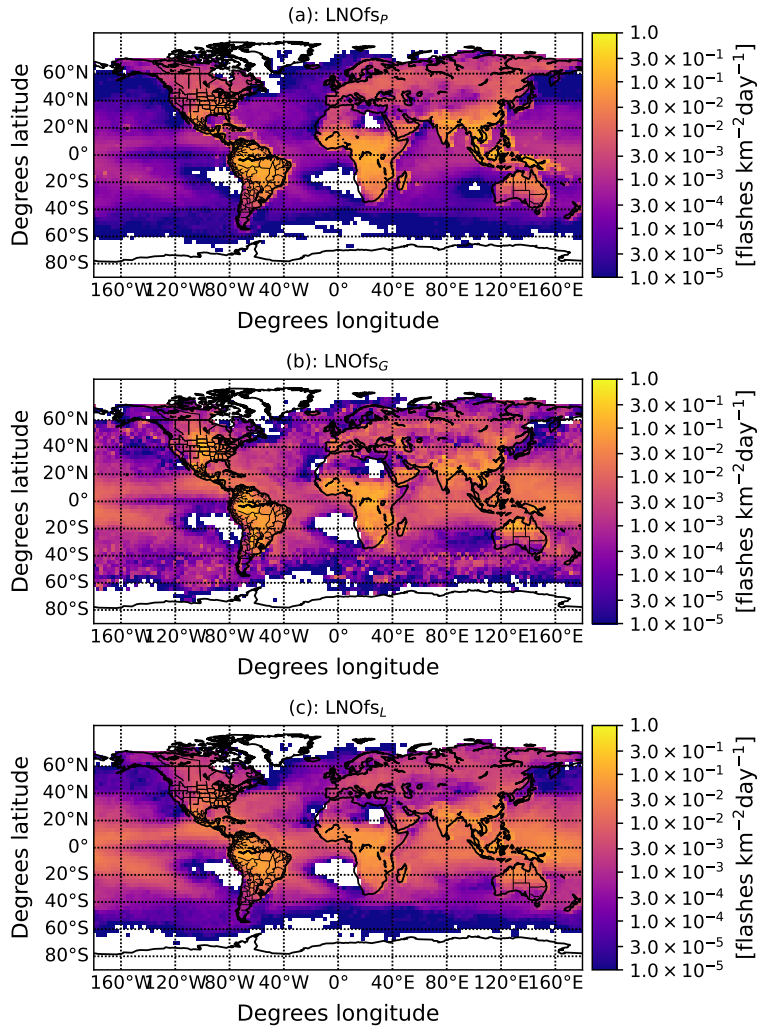


**Figure S1.** Simulated annual average flash density between 1 January 2001 and 31 December 2001 using different lightning parameterizations in the LNOfs simulations. The subscript indicates the used lightning parameterization: *P*: Price and Rind (1992) (a), *G*: Grewe et al. (2001) (b), and *L*: Luhar et al. (2021) (c).

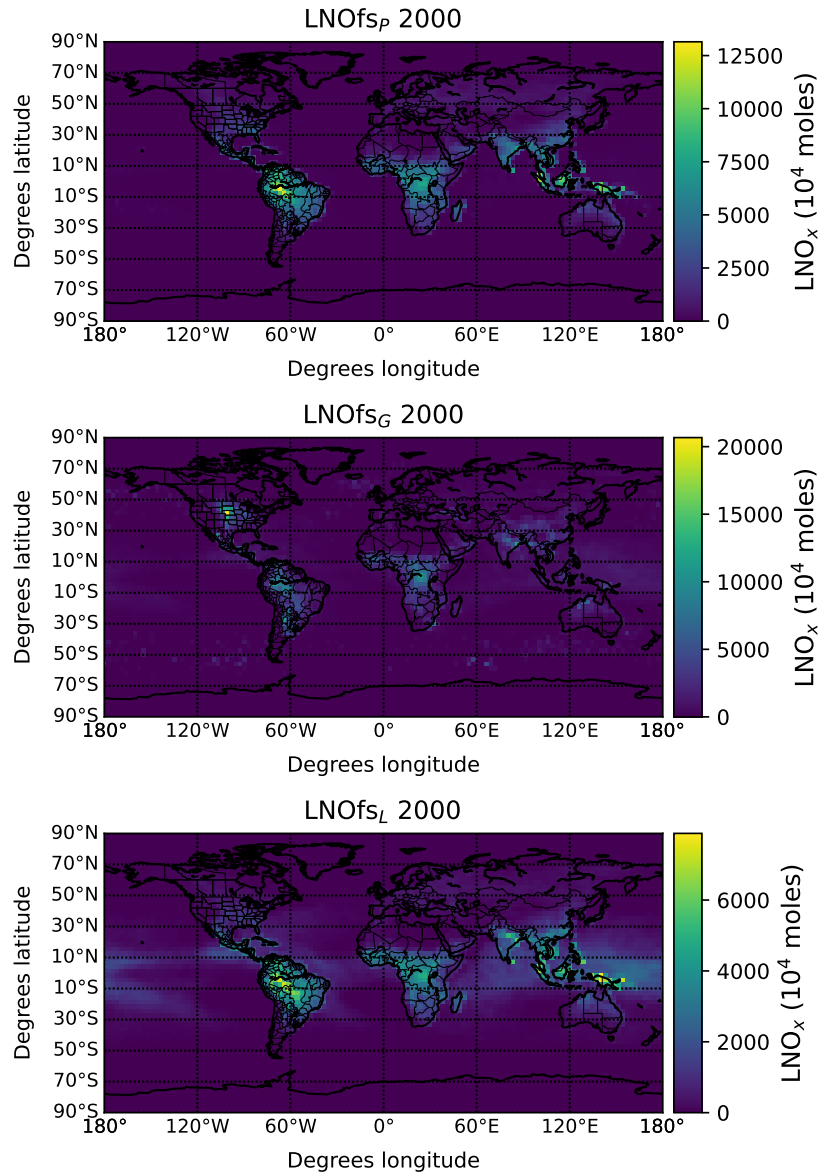


**Figure S2.** Comparison of spatial distribution of the mean monthly  $\text{LNO}_x$  during 2000 between the  $\text{LNOfs}$  simulations. The subscript indicates the used lightning parameterization:  $P$ : Price and Rind (1992),  $G$ : Grawe et al. (2001), and  $L$ : Luhan et al. (2021).

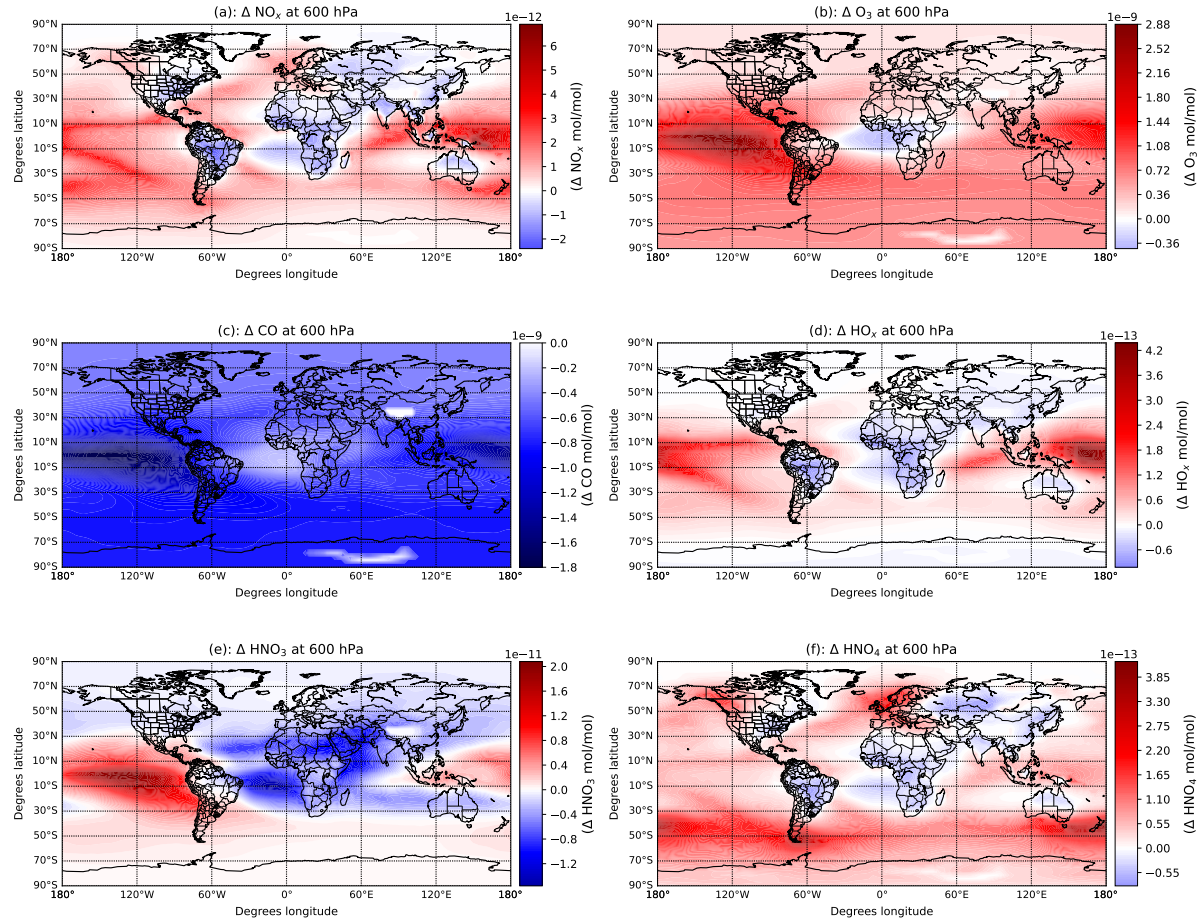


**Figure S3.** Annually (2002–2007) and globally averaged differences of the NO<sub>x</sub>, O<sub>3</sub>, CO, HO<sub>x</sub>, HNO<sub>3</sub> and HNO<sub>4</sub> mixing ratios between the simulation with the LNO<sub>x</sub> based on the flash frequency (LNOfs<sub>P</sub>) and the simulation with a constant quantity of the LNO<sub>x</sub> per flash (CTR<sub>P</sub>) at 600 hPa vertical levels.

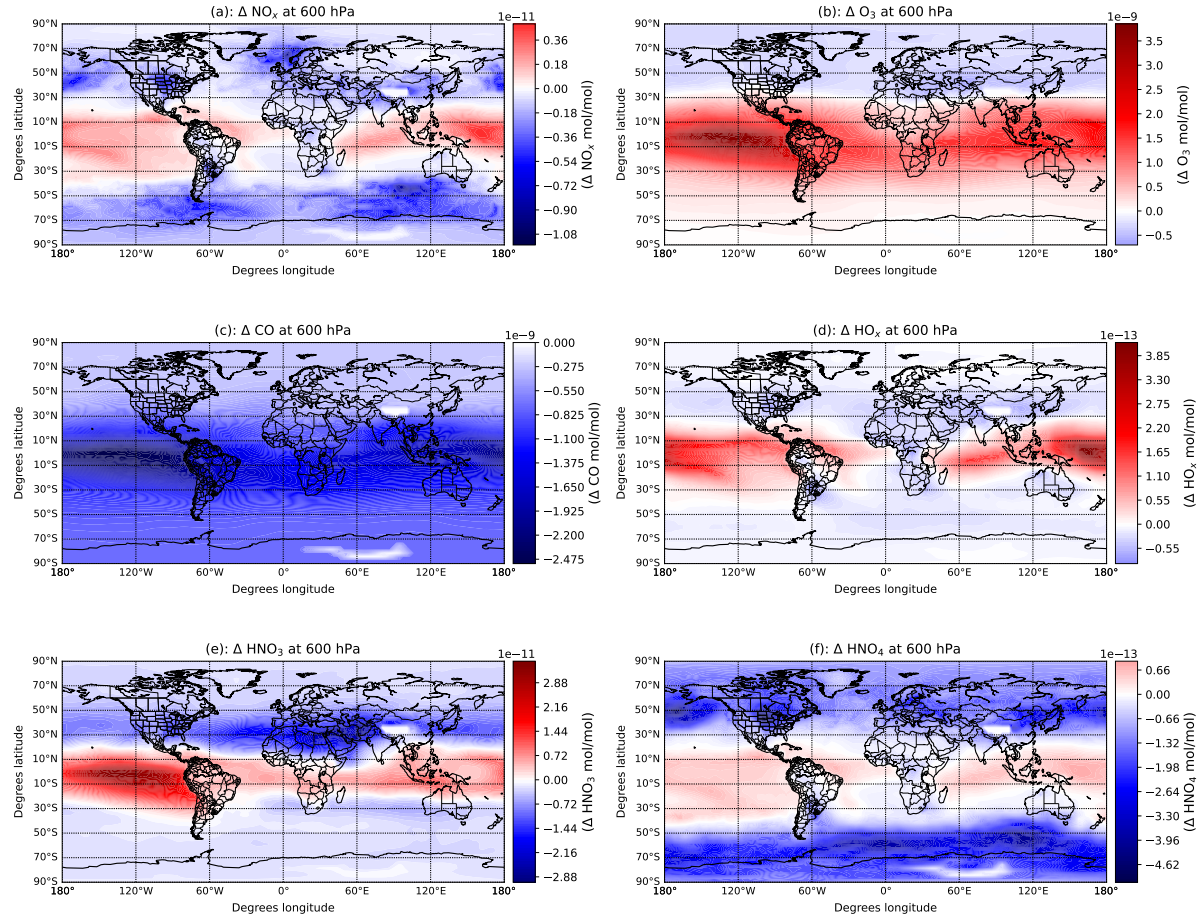


**Figure S4.** Annually (2002-2007) and globally averaged differences of the  $\text{NO}_x$ ,  $\text{O}_3$ ,  $\text{CO}$ ,  $\text{HO}_x$ ,  $\text{HNO}_3$  and  $\text{HNO}_4$  mixing ratios between the simulation with the  $\text{LNO}_x$  based on the flash frequency ( $\text{LNOfs}_G$ ) and the simulation with a constant quantity of the  $\text{LNO}_x$  per flash ( $\text{CTR}_G$ ) at 600 hPa vertical levels.

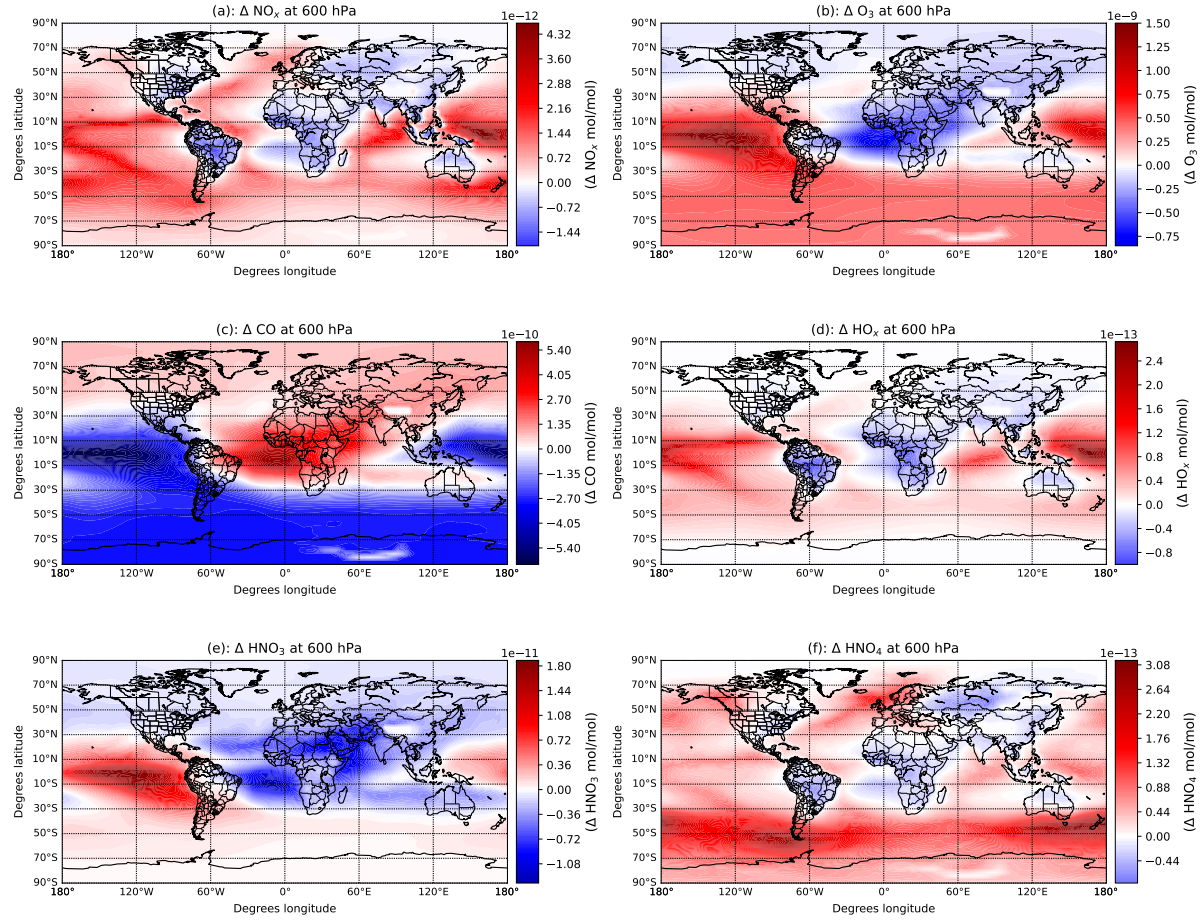


**Figure S5.** Annually (2002–2007) and globally averaged differences of the  $\text{NO}_x$ ,  $\text{O}_3$ ,  $\text{CO}$ ,  $\text{HO}_x$ ,  $\text{HNO}_3$  and  $\text{HNO}_4$  mixing ratios between the simulation with the  $\text{LNO}_x$  based on the flash frequency ( $\text{LNOfs}_L$ ) and the simulation with a constant quantity of the  $\text{LNO}_x$  per flash ( $\text{CTR}_L$ ) at 600 hPa vertical levels.

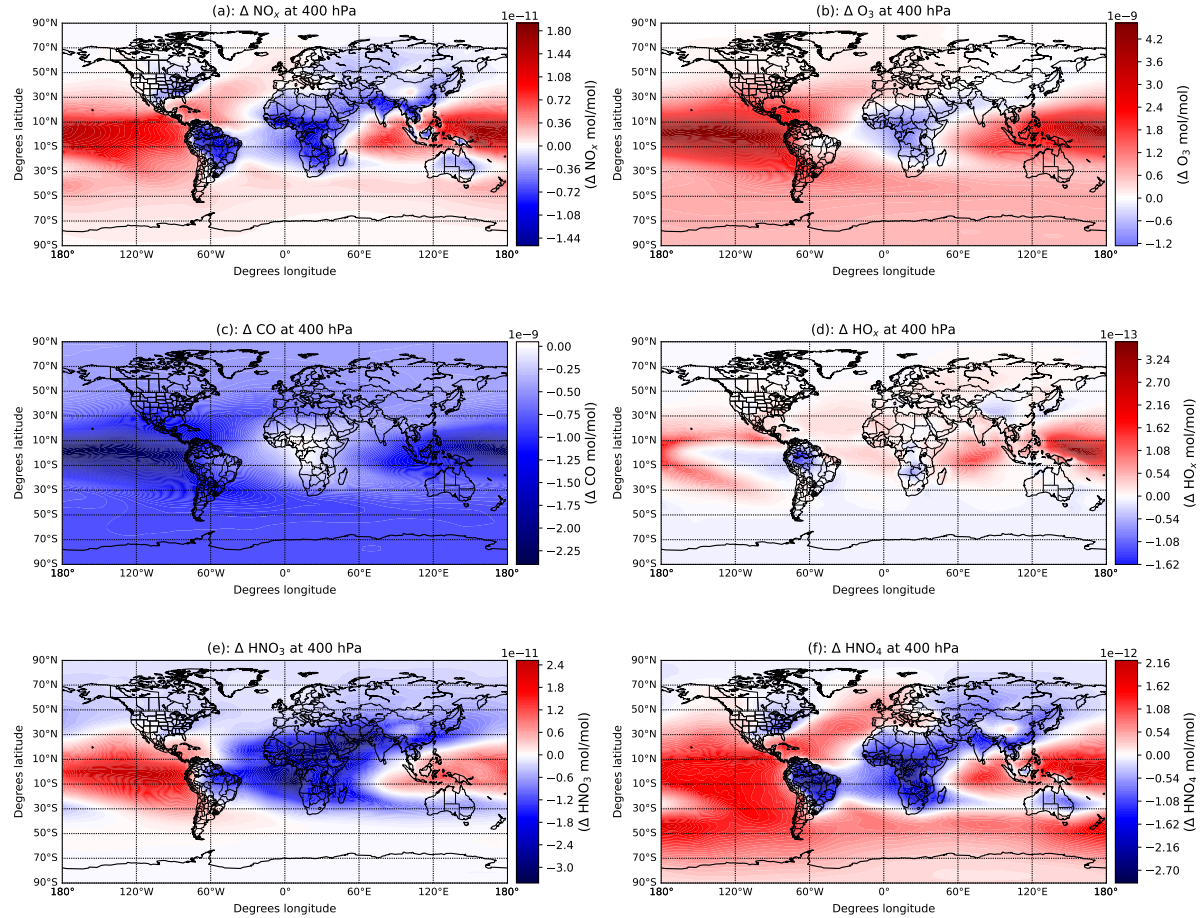


**Figure S6.** Annually (2002-2007) and globally averaged differences of the  $\text{NO}_x$ ,  $\text{O}_3$ ,  $\text{CO}$ ,  $\text{HO}_x$ ,  $\text{HNO}_3$  and  $\text{HNO}_4$  mixing ratios between the simulation with the  $\text{LNO}_x$  based on the flash frequency ( $\text{LNOfs}_P$ ) and the simulation with a constant quantity of the  $\text{LNO}_x$  per flash ( $\text{CTR}_P$ ) at 400 hPa vertical levels.

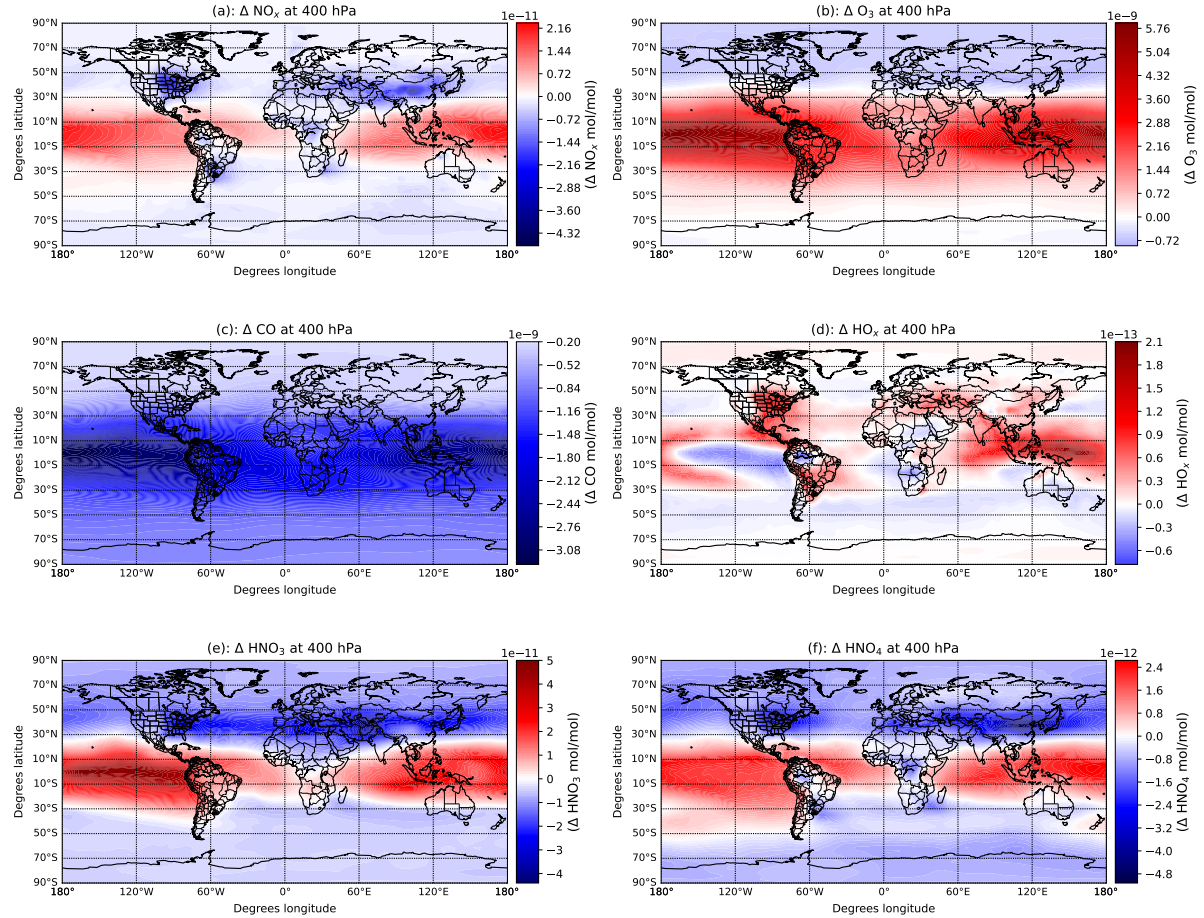


**Figure S7.** Annually (2002–2007) and globally averaged differences of the  $\text{NO}_x$ ,  $\text{O}_3$ ,  $\text{CO}$ ,  $\text{HO}_x$ ,  $\text{HNO}_3$  and  $\text{HNO}_4$  mixing ratios between the simulation with the  $\text{LNO}_x$  based on the flash frequency ( $\text{LNOfs}_G$ ) and the simulation with a constant quantity of the  $\text{LNO}_x$  per flash ( $\text{CTR}_G$ ) at 400 hPa vertical levels.

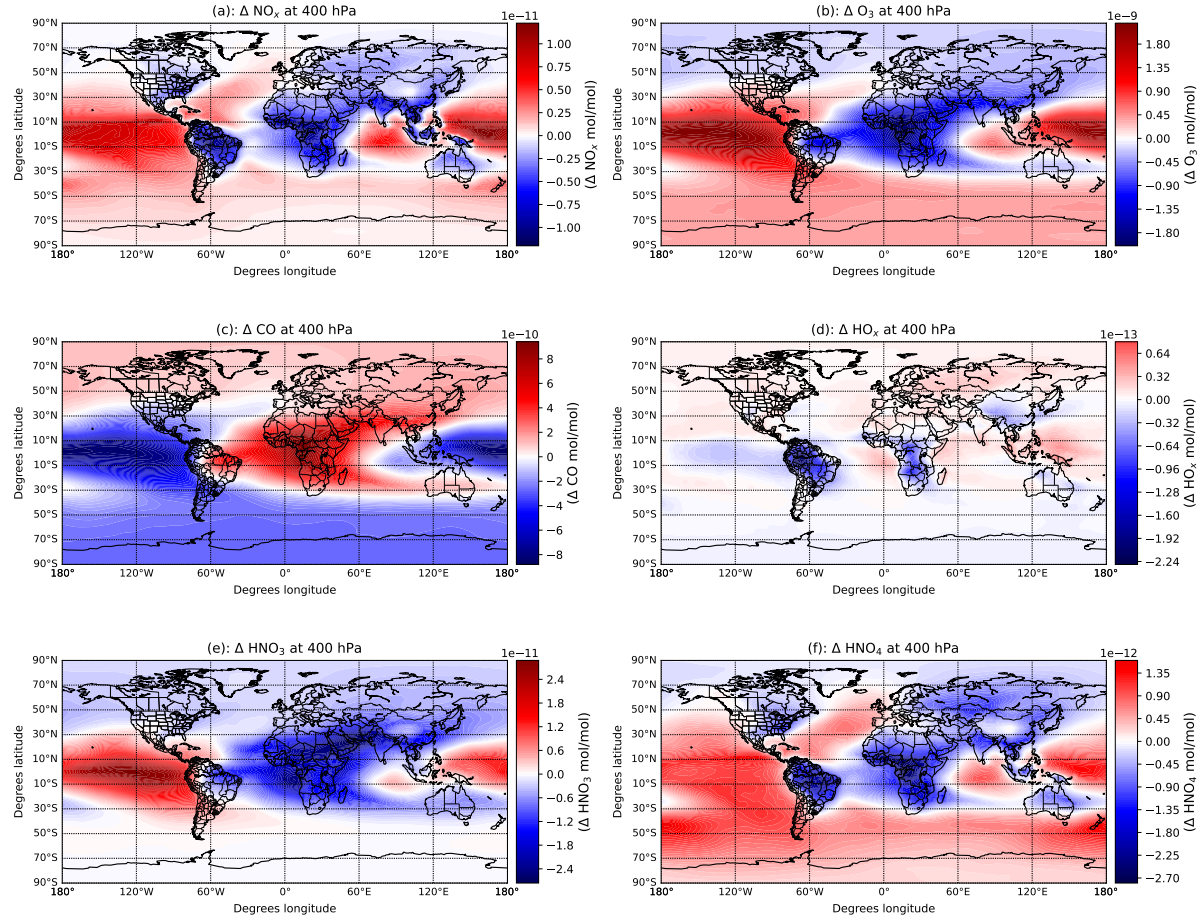


**Figure S8.** Annually (2002-2007) and globally averaged differences of the  $\text{NO}_x$ ,  $\text{O}_3$ ,  $\text{CO}$ ,  $\text{HO}_x$ ,  $\text{HNO}_3$  and  $\text{HNO}_4$  mixing ratios between the simulation with the  $\text{LNO}_x$  based on the flash frequency ( $\text{LNOfs}_L$ ) and the simulation with a constant quantity of the  $\text{LNO}_x$  per flash ( $\text{CTR}_L$ ) at 400 hPa vertical levels.

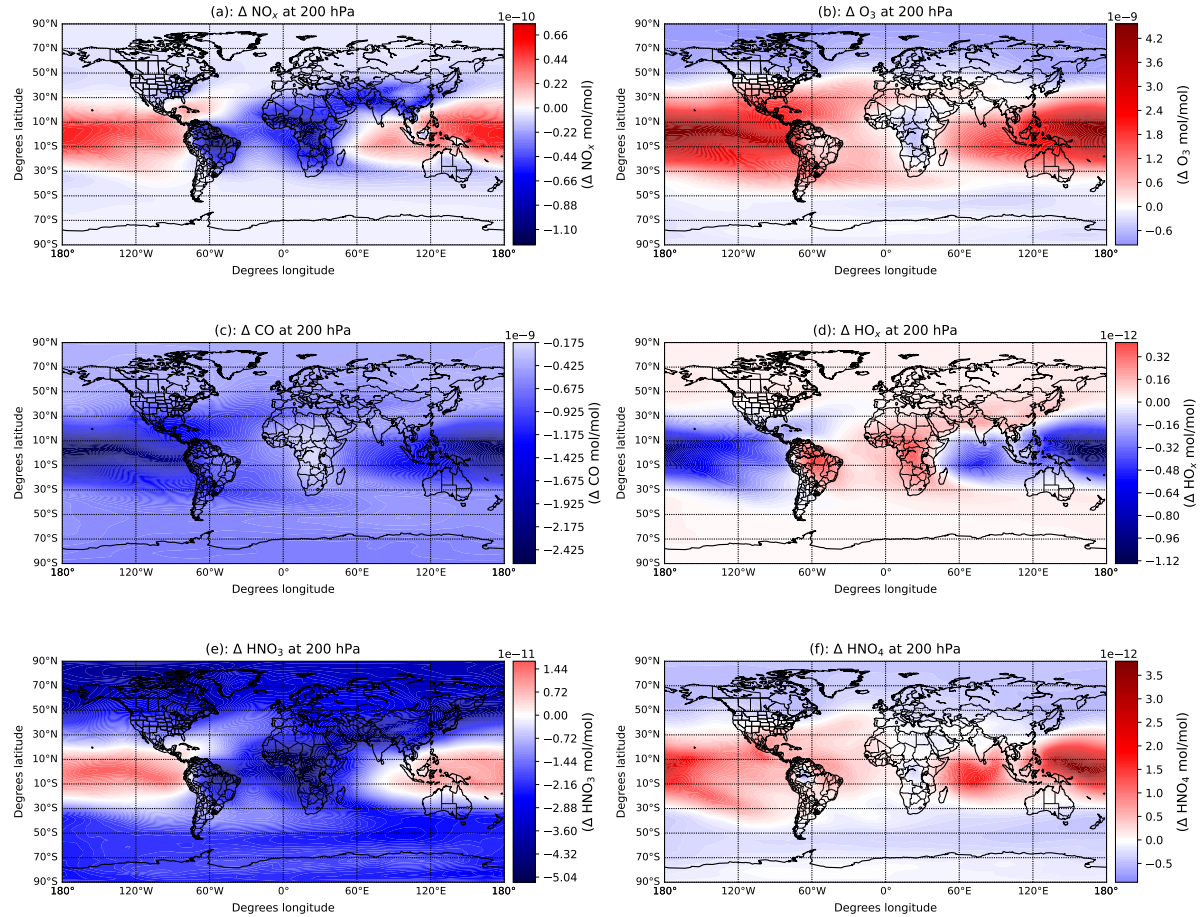


**Figure S9.** Annually (2002-2007) and globally averaged differences of the  $\text{NO}_x$ ,  $\text{O}_3$ ,  $\text{CO}$ ,  $\text{HO}_x$ ,  $\text{HNO}_3$  and  $\text{HNO}_4$  mixing ratios between the simulation with the  $\text{LNO}_x$  based on the flash frequency ( $\text{LNOfs}_P$ ) and the simulation with a constant quantity of the  $\text{LNO}_x$  per flash ( $\text{CTR}_P$ ) at 200 hPa vertical levels.

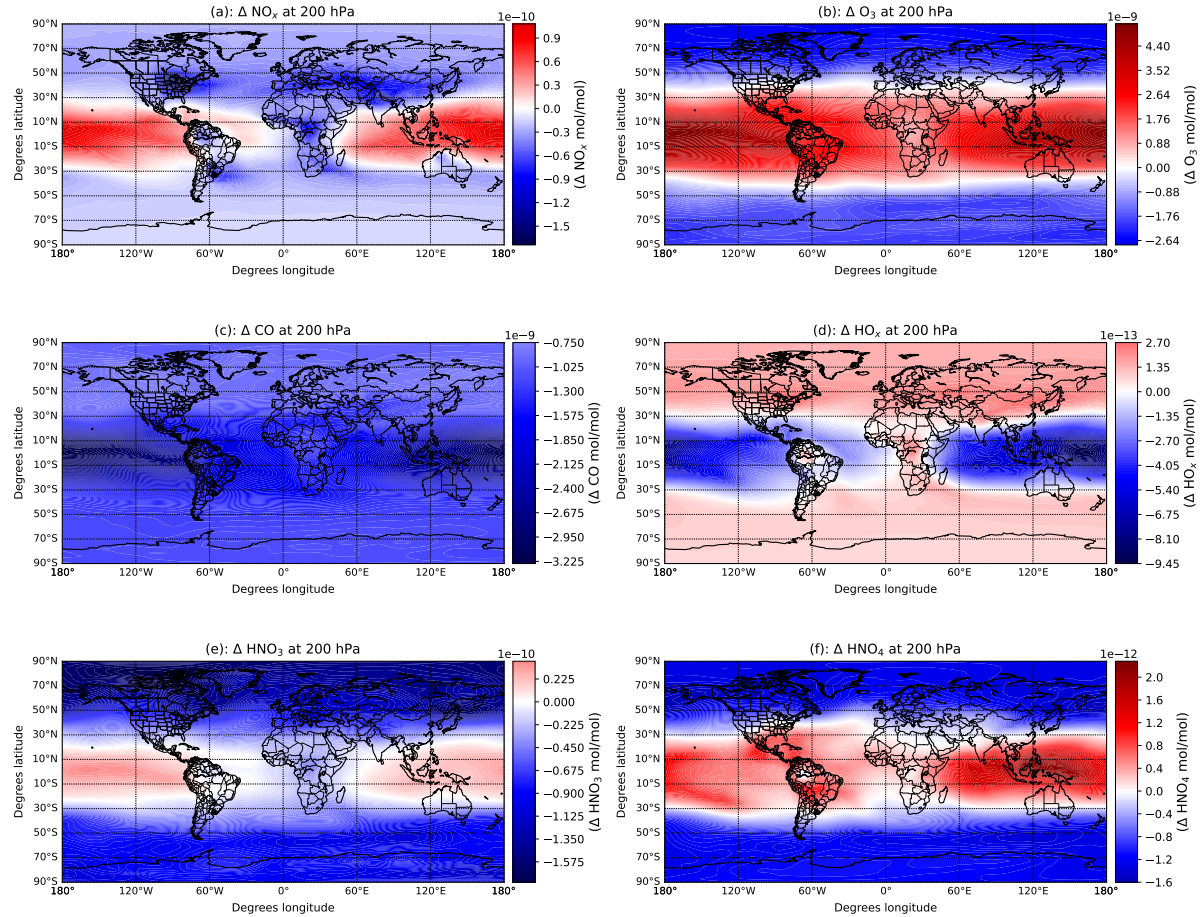


**Figure S10.** Annually (2002-2007) and globally averaged differences of the  $\text{NO}_x$ ,  $\text{O}_3$ ,  $\text{CO}$ ,  $\text{HO}_x$ ,  $\text{HNO}_3$  and  $\text{HNO}_4$  mixing ratios between the simulation with the  $\text{LNO}_x$  based on the flash frequency ( $\text{LNOfs}_G$ ) and the simulation with a constant quantity of the  $\text{LNO}_x$  per flash ( $\text{CTR}_G$ ) at 200 hPa vertical levels.

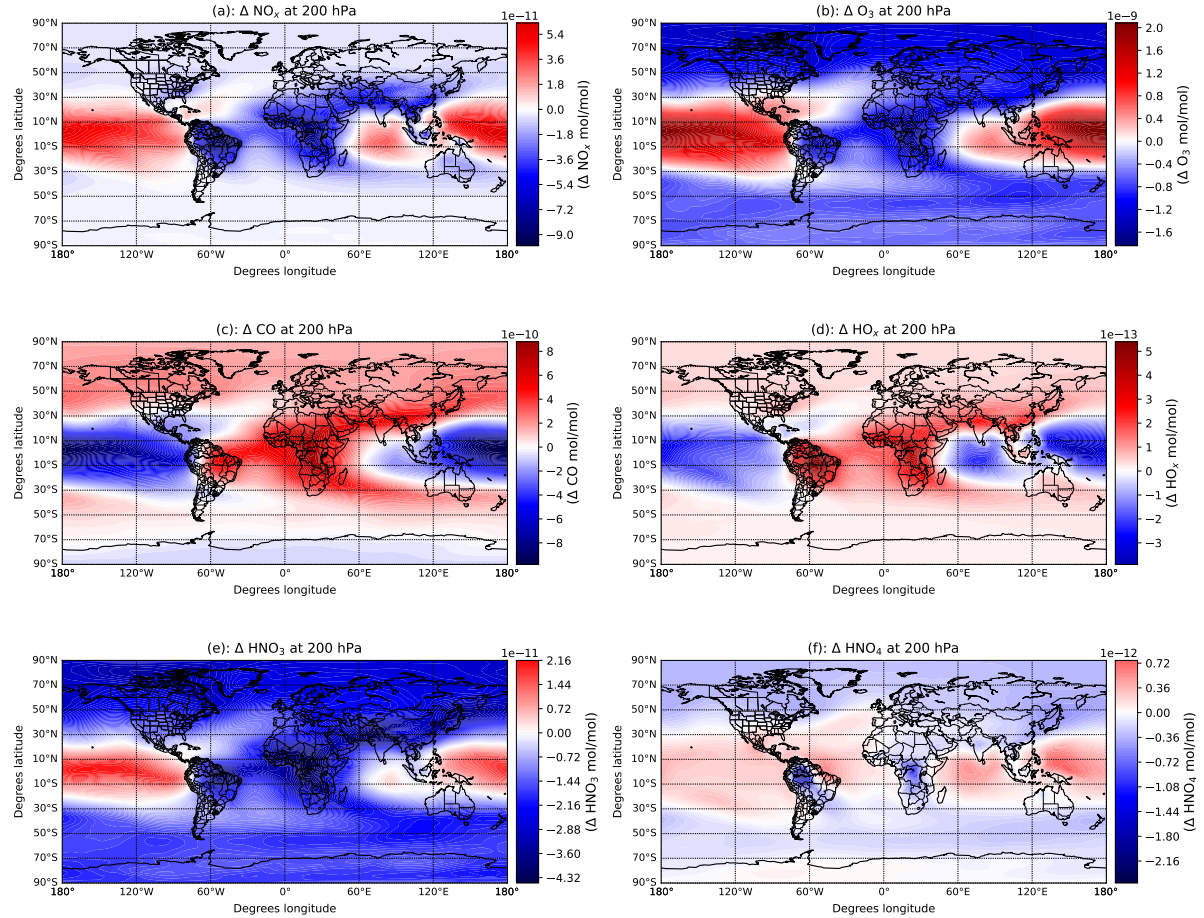


**Figure S11.** Annually (2002-2007) and globally averaged differences of the  $\text{NO}_x$ ,  $\text{O}_3$ ,  $\text{CO}$ ,  $\text{HO}_x$ ,  $\text{HNO}_3$  and  $\text{HNO}_4$  mixing ratios between the simulation with the  $\text{LNO}_x$  based on the flash frequency ( $\text{LNOfs}_L$ ) and the simulation with a constant quantity of the  $\text{LNO}_x$  per flash ( $\text{CTR}_L$ ) at 200 hPa vertical levels.

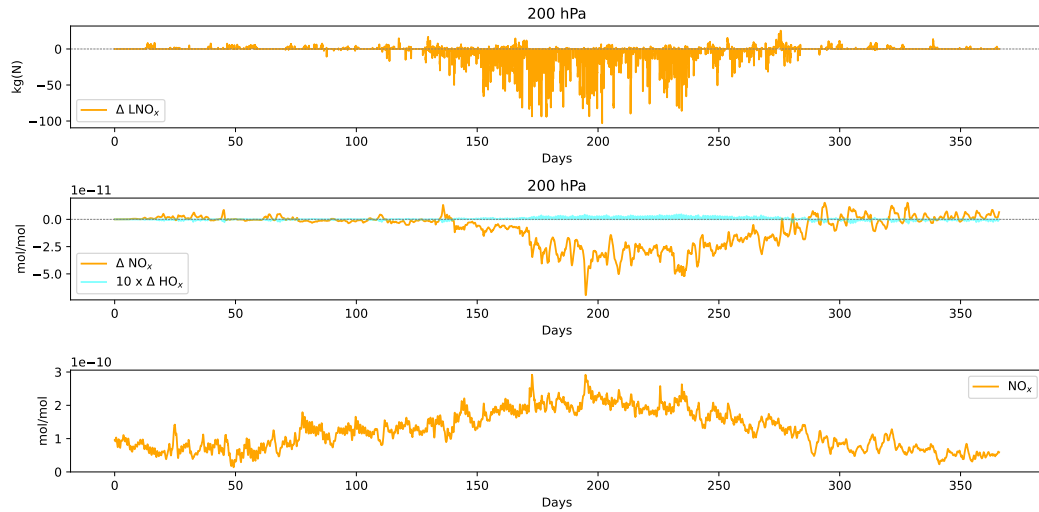


**Figure S12.** (Upper panel): Difference of the hourly total column injection of  $\text{LNO}_x$  between the LNOfs<sub>L</sub> and CTR<sub>L</sub> simulations over a 1-year period (day 1 corresponds to 1 January, 2000). (Middle panel): Hourly differences of the  $\text{NO}_x$  and  $\text{HO}_x$  mixing ratios at 200 hPa. (Lower panel): Hourly background mixing ratio of  $\text{NO}_x$  at the 200 hPa level in the LNOfs<sub>L</sub> simulation. The three panels correspond to a spatial average over Europe (bounded by  $42^{\circ}\text{N}$  and  $52^{\circ}\text{N}$  latitude degrees, and  $0^{\circ}$  to  $24^{\circ}\text{E}$  longitude degrees).

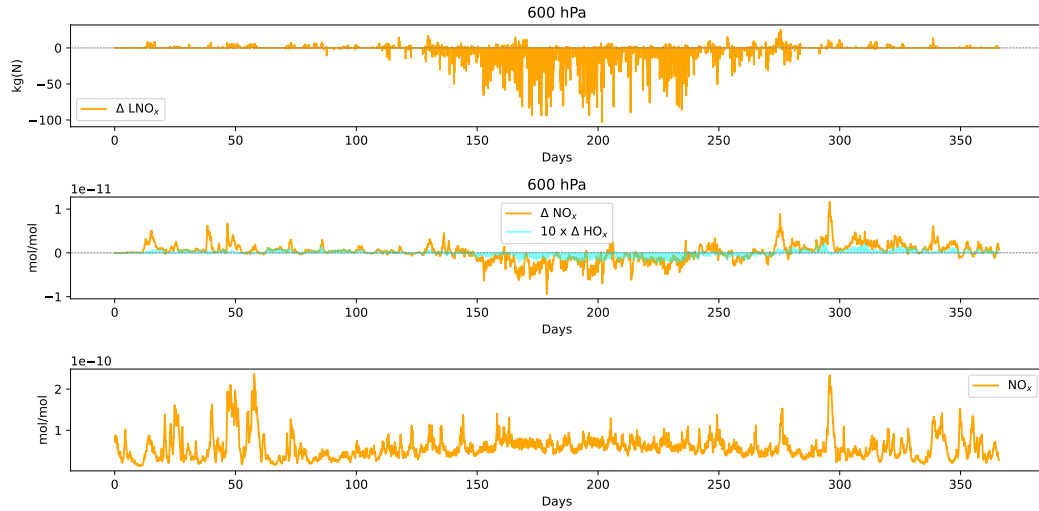


**Figure S13.** (Upper panel): Difference of the hourly total column injection of  $\text{LNO}_x$  between the LNOfs<sub>L</sub> and CTR<sub>L</sub> simulations over a 1-year period (day 1 corresponds to 1 January, 2000). (Middle panel): Hourly differences of the  $\text{NO}_x$  and  $\text{HO}_x$  mixing ratios at 600 hPa. (Lower panel): Hourly background mixing ratio of  $\text{NO}_x$  at the 600 hPa level in the LNOfs<sub>L</sub> simulation. The three panels correspond to a spatial average over Europe (bounded by  $42^{\circ}\text{N}$  and  $52^{\circ}\text{N}$  latitude degrees, and  $0^{\circ}$  to  $24^{\circ}\text{E}$  longitude degrees).

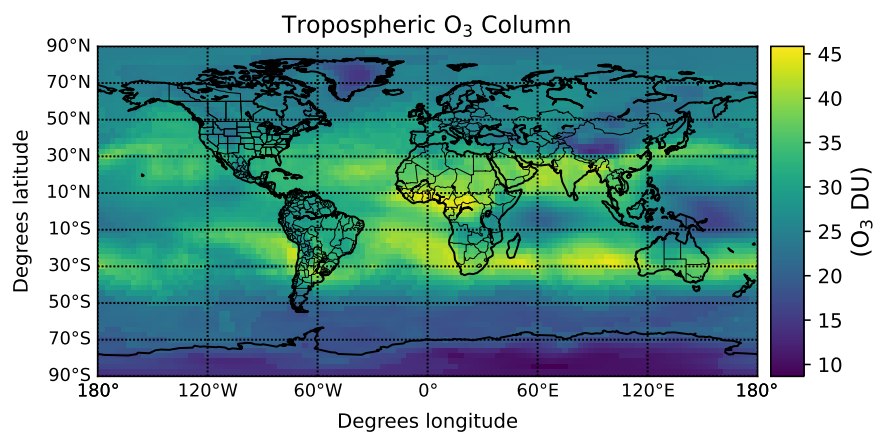


**Figure S14.** Monthly (January 2004) and globally averaged tropospheric O<sub>3</sub> column in the CTR simulation, including the parameterization of lightning by Grewe et al. (2001) and a constant quantity of the LNO<sub>x</sub> per flash (Price et al., 1997).

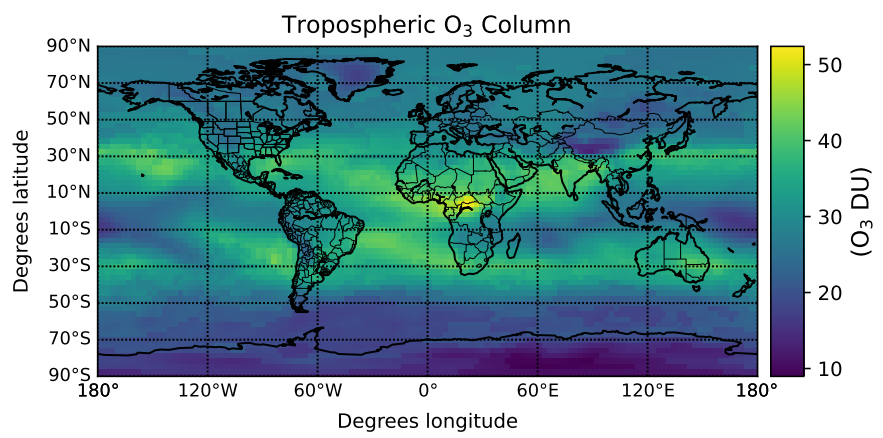


**Figure S15.** Monthly (February 2004) and globally averaged tropospheric O<sub>3</sub> column in the CTR simulation, including the parameterization of lightning by Grewe et al. (2001) and a constant quantity of the LNO<sub>x</sub> per flash (Price et al., 1997).

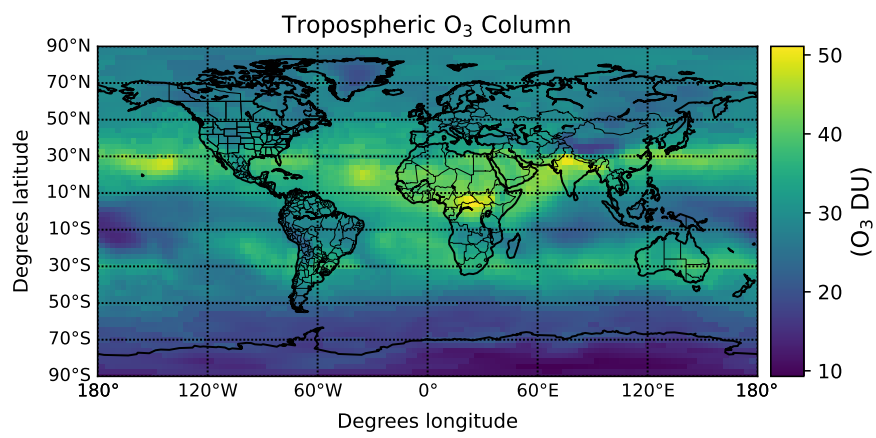


**Figure S16.** Monthly (March 2004) and globally averaged tropospheric O<sub>3</sub> column in the CTR simulation, including the parameterization of lightning by Grewe et al. (2001) and a constant quantity of the LNO<sub>x</sub> per flash (Price et al., 1997).

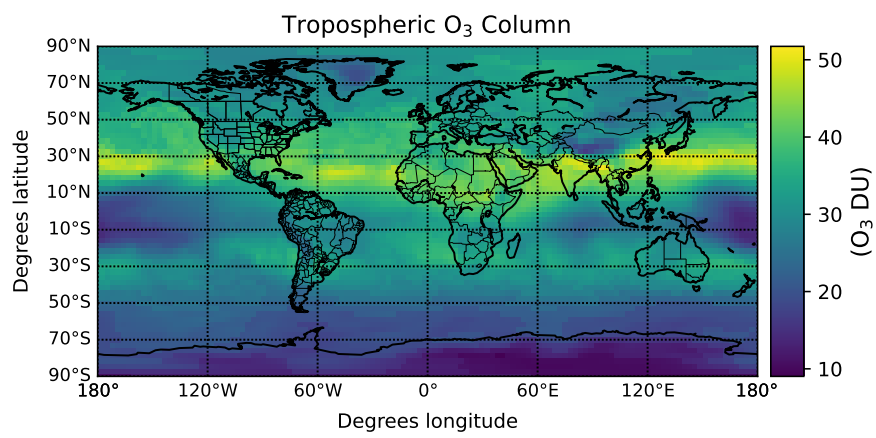


**Figure S17.** Monthly (April 2004) and globally averaged tropospheric O<sub>3</sub> column in the CTR simulation, including the parameterization of lightning by Grewe et al. (2001) and a constant quantity of the LNO<sub>x</sub> per flash (Price et al., 1997).

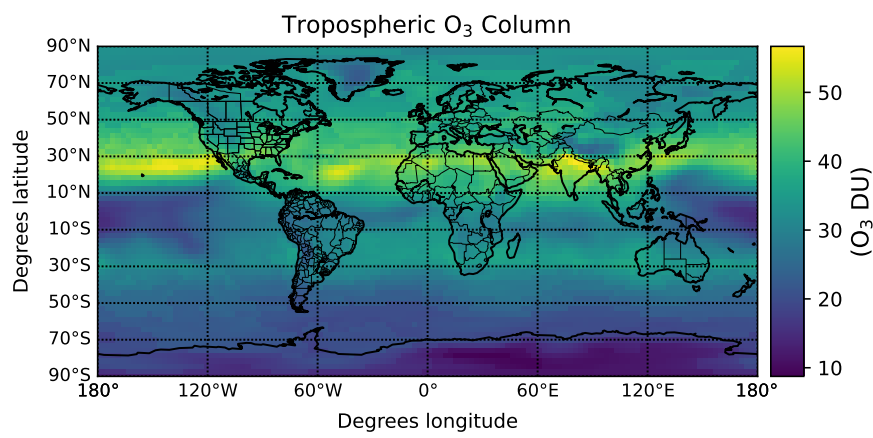


**Figure S18.** Monthly (May 2004) and globally averaged tropospheric O<sub>3</sub> column in the CTR simulation, including the parameterization of lightning by Grewe et al. (2001) and a constant quantity of the LNO<sub>x</sub> per flash (Price et al., 1997).

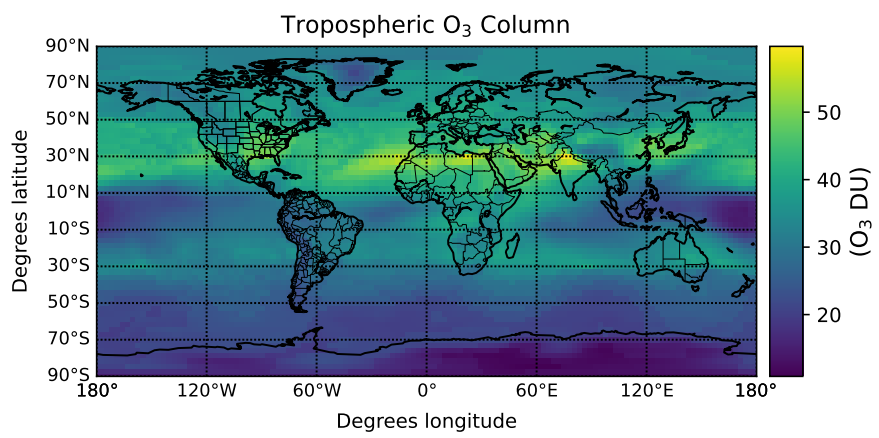


**Figure S19.** Monthly (June 2004) and globally averaged tropospheric O<sub>3</sub> column in the CTR simulation, including the parameterization of lightning by Grewe et al. (2001) and a constant quantity of the LNO<sub>x</sub> per flash (Price et al., 1997).

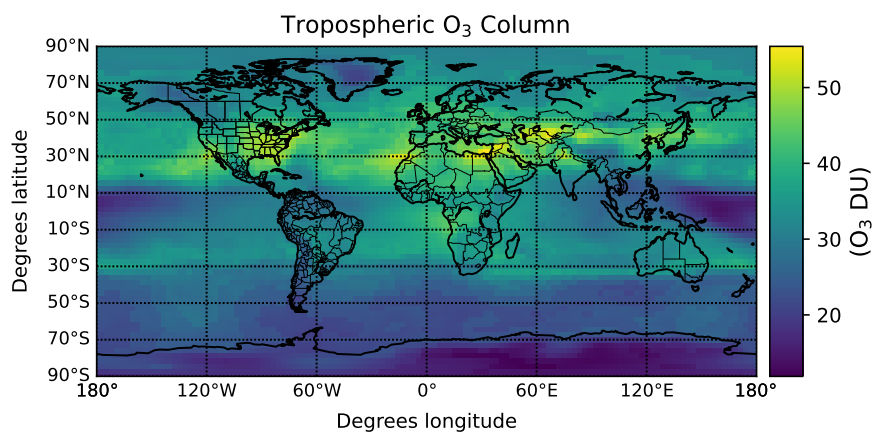


**Figure S20.** Monthly (July 2004) and globally averaged tropospheric O<sub>3</sub> column in the CTR simulation, including the parameterization of lightning by Grewe et al. (2001) and a constant quantity of the LNO<sub>x</sub> per flash (Price et al., 1997).

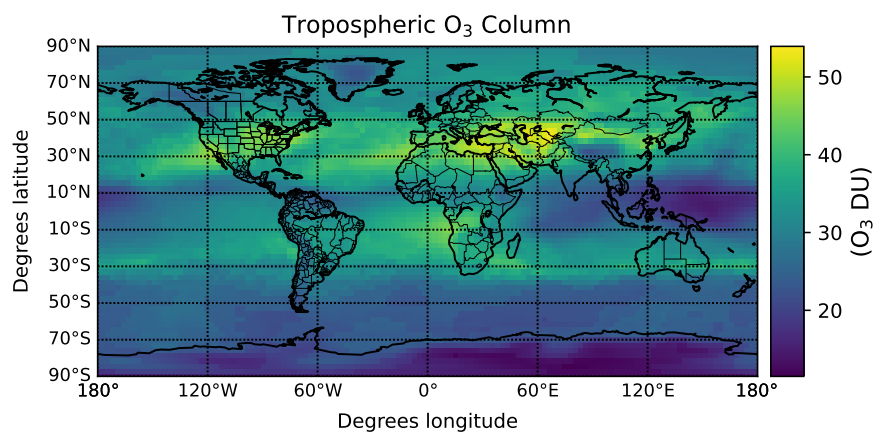


**Figure S21.** Monthly (August 2004) and globally averaged tropospheric O<sub>3</sub> column in the CTR simulation, including the parameterization of lightning by Grewe et al. (2001) and a constant quantity of the LNO<sub>x</sub> per flash (Price et al., 1997).

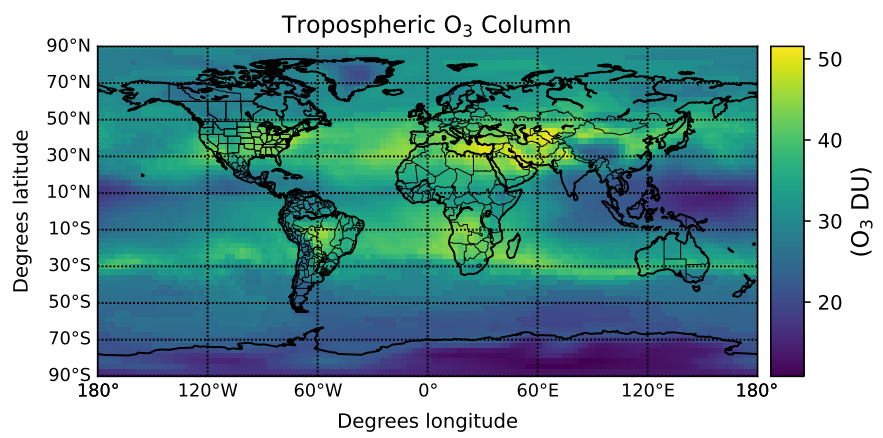


**Figure S22.** Monthly (September 2004) and globally averaged tropospheric O<sub>3</sub> column in the CTR simulation, including the parameterization of lightning by Grewe et al. (2001) and a constant quantity of the LNO<sub>x</sub> per flash (Price et al., 1997).

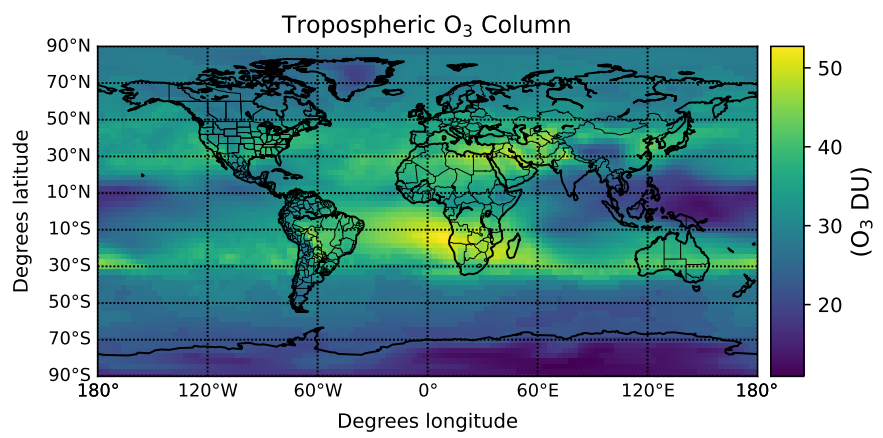


**Figure S23.** Monthly (October 2004) and globally averaged tropospheric O<sub>3</sub> column in the CTR simulation, including the parameterization of lightning by Grewe et al. (2001) and a constant quantity of the LNO<sub>x</sub> per flash (Price et al., 1997).

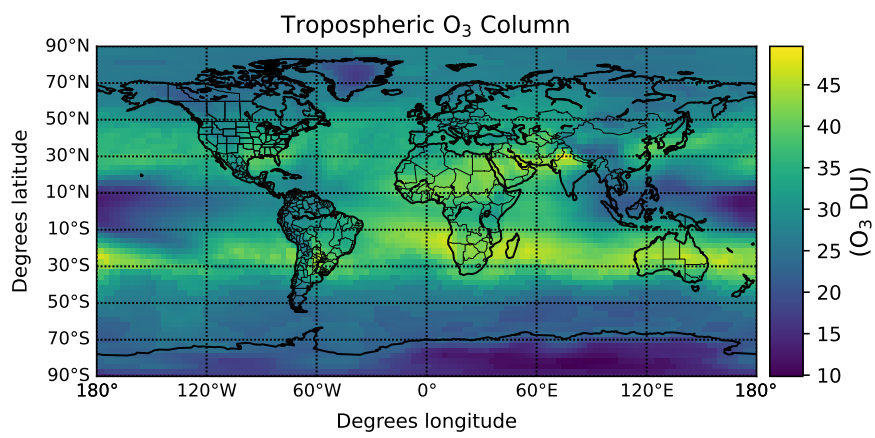


**Figure S24.** Monthly (November 2004) and globally averaged tropospheric O<sub>3</sub> column in the CTR simulation, including the parameterization of lightning by Grewe et al. (2001) and a constant quantity of the LNO<sub>x</sub> per flash (Price et al., 1997).

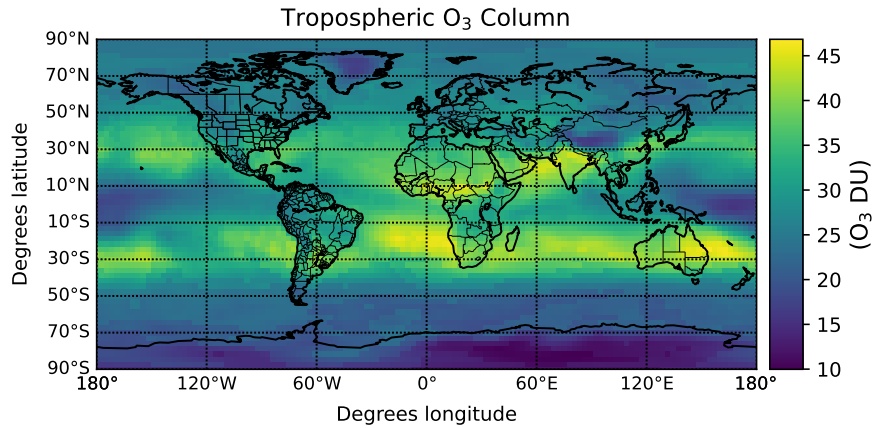


**Figure S25.** Monthly (December 2004) and globally averaged tropospheric O<sub>3</sub> column in the CTR simulation, including the parameterization of lightning by Grewe et al. (2001) and a constant quantity of the LNO<sub>x</sub> per flash (Price et al., 1997).

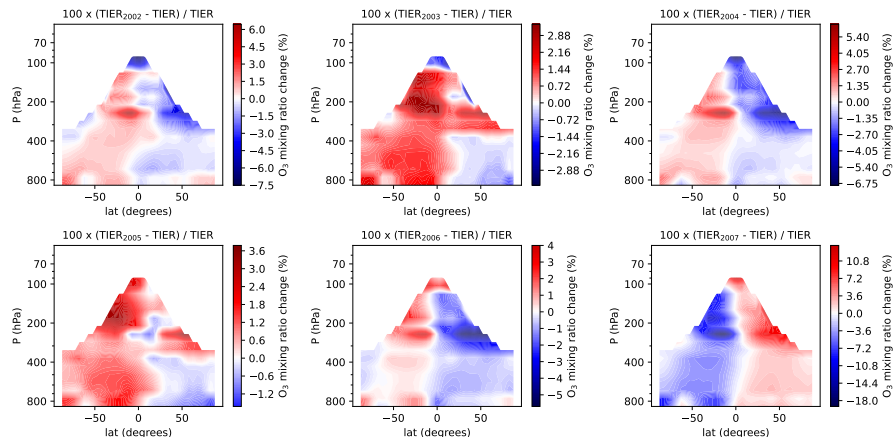


**Figure S26.** Interannual zonally averaged differences (in %) during DJF of the vertical O<sub>3</sub> mixing ratio between the annual Bodeker scientific global vertically resolved ozone database Tier 1.4 vn1.0 product Hassler et al. (2009) and the annually mean during the period 2002-2007. The border to the white region represents the zonally averaged mean altitude of the climatological tropopause.

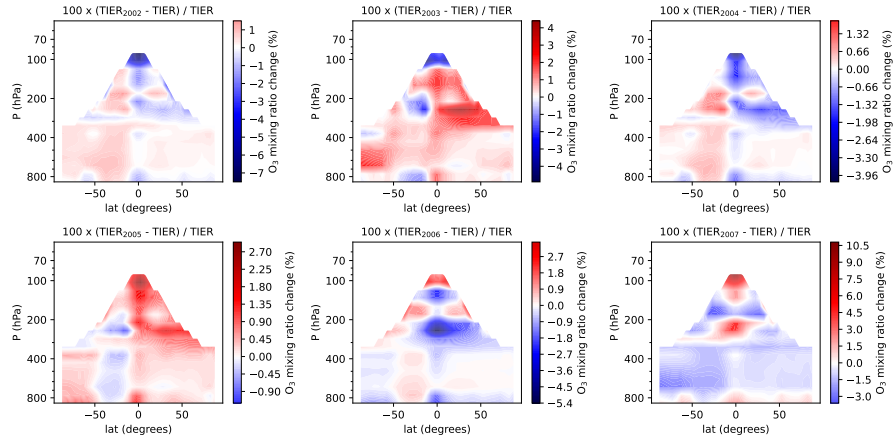


**Figure S27.** Interannual zonally averaged differences (in %) during MAM of the vertical O<sub>3</sub> mixing ratio between the annual Bodeker scientific global vertically resolved ozone database Tier 1.4 vn1.0 product Hassler et al. (2009) and the annually mean during the period 2002-2007. The border to the white region represents the zonally averaged mean altitude of the climatological tropopause.

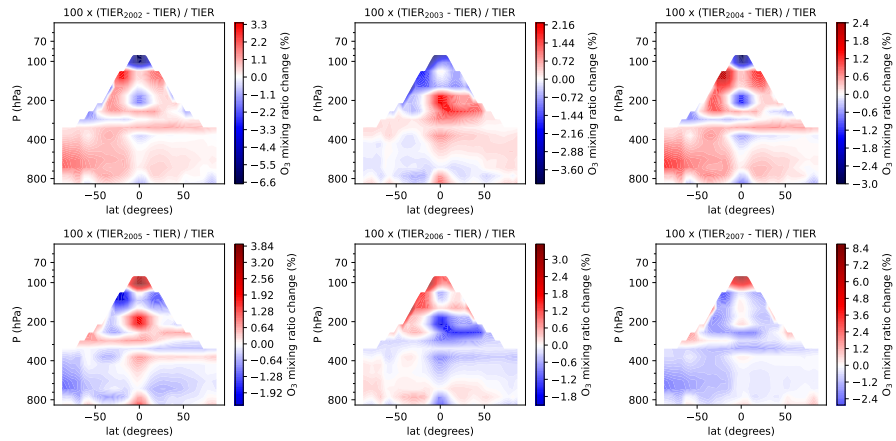


**Figure S28.** Interannual zonally averaged differences (in %) during JJA of the vertical O<sub>3</sub> mixing ratio between the annual Bodeker scientific global vertically resolved ozone database Tier 1.4 vn1.0 product Hassler et al. (2009) and the annually mean during the period 2002-2007. The border to the white region represents the zonally averaged mean altitude of the climatological tropopause.

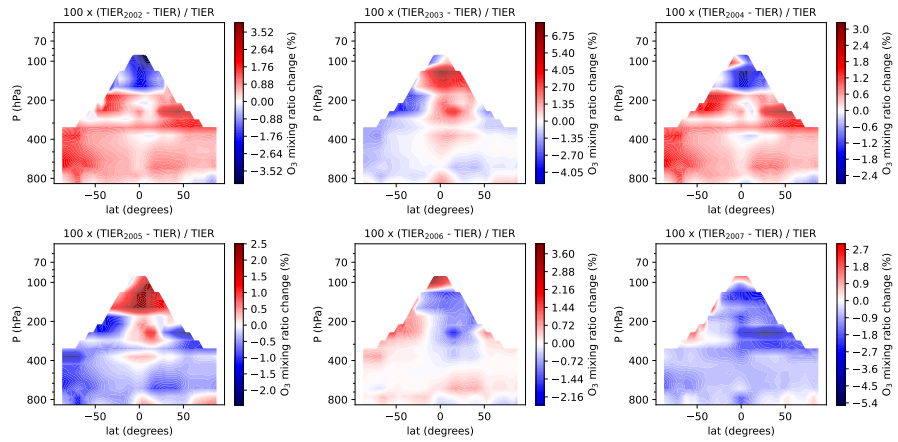


**Figure S29.** Interannual zonally averaged differences (in %) during SON of the vertical O<sub>3</sub> mixing ratio between the annual Bodeker scientific global vertically resolved ozone database Tier 1.4 vn1.0 product Hassler et al. (2009) and the annually mean during the period 2002-2007. The border to the white region represents the zonally averaged mean altitude of the climatological tropopause.

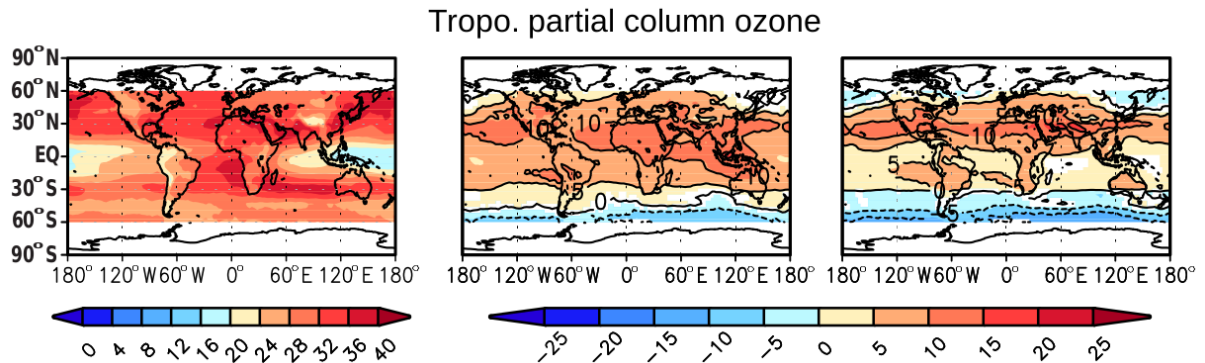


**Figure S30.** Left column: climatological annual mean of observed tropospheric partial column ozone (AURA Microwave Limb Sounder/Ozone Monitoring Instrument (MLS/OMI), Ziemke et al. (2011))), all in DU. The analyses cover the years 2005 to 2011. Middle column: differences between the RC1-base-07 simulation and the observations. Right column: same as middle column, but for the RC1SD-base-07 simulation. Statistically significant changes on the 95% confidence level are coloured. This figure is adapted from (Jöckel et al., 2016, Fig. 29).

## 15 References

- Bucsela, E. J., Pickering, K. E., Allen, D. J., Holzworth, R. H., and Krotkov, N. A.: Midlatitude lightning NO<sub>x</sub> production efficiency inferred from OMI and WWLLN data, *J. Geophys. Res. Atmos.*, 124, 13 475–13 497, <https://doi.org/10.1029/2019JD030561>, 2019.
- Greve, V., Brunner, D., Dameris, M., Grenfell, J., Hein, R., Shindell, D., and Staehelin, J.: Origin and variability of upper tropospheric nitrogen oxides and ozone at northern mid-latitudes, *Atmos. Environ.*, 35, 3421–3433, [https://doi.org/10.1016/S1352-2310\(01\)00134-0](https://doi.org/10.1016/S1352-2310(01)00134-0), 2001.
- Hassler, B., Bodeker, G., Cionni, I., and Dameris, M.: A vertically resolved, monthly mean, ozone database from 1979 to 2100 for constraining global climate model simulations, *Int. J. Remote Sens.*, 30, 4009–4018, 2009.
- Jöckel, P., Tost, H., Pozzer, A., Kunze, M., Kirner, O., Brenninkmeijer, C. A., Brinkop, S., Cai, D. S., Dyroff, C., Eckstein, J., et al.: Earth system chemistry integrated modelling (ESCiMo) with the modular earth submodel system (MESSy) version 2.51, *Geosci. Model. Dev.*, 9, 1153–1200, <https://doi.org/10.5194/gmd-9-1153-2016>, 2016.
- Luhar, A. K., Galbally, I. E., Woodhouse, M. T., and Abraham, N. L.: Assessing and improving cloud-height-based parameterisations of global lightning flash rate, and their impact on lightning-produced NO<sub>x</sub> and tropospheric composition in a chemistry–climate model, *Atmos. Chem. Phys.*, 21, 7053–7082, <https://doi.org/10.5194/acp-21-7053-2021>, 2021.
- Price, C. and Rind, D.: A simple lightning parameterization for calculating global lightning distributions, *J. Geophys. Res.*, 97, 9919, <https://doi.org/10.1029/92JD00719>, 1992.
- Price, C., Penner, J., and Prather, M.: NO<sub>x</sub> from lightning: 1. Global distribution based on lightning physics, *J. Geophys. Res.*, 102, 5929, <https://doi.org/10.1029/96JD03504>, 1997.
- Ziemke, J., Chandra, S., Labow, G., Bhartia, P., Froidevaux, L., and Witte, J.: A global climatology of tropospheric and stratospheric ozone derived from Aura OMI and MLS measurements, *Atmos. Chem. Phys.*, 11, 9237–9251, <https://doi.org/10.5194/acp-11-9237-2011>, 2011.